

# Reactivity of Biarylazacyclooctynones in Copper-Free Click Chemistry

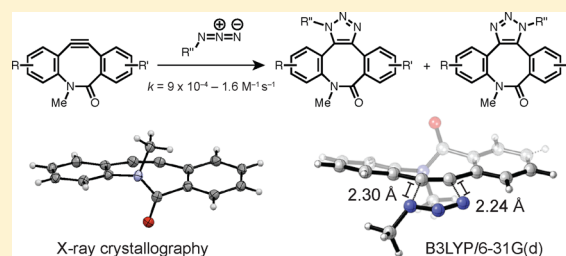
Chelsea G. Gordon,<sup>†</sup> Joel L. Mackey,<sup>‡</sup> John C. Jewett,<sup>†,‡,§</sup> Ellen M. Sletten,<sup>†</sup> K. N. Houk,<sup>\*,‡</sup> and Carolyn R. Bertozzi<sup>\*,†,‡,§</sup>

<sup>†</sup>Departments of Chemistry and <sup>‡</sup>Molecular and Cell Biology and <sup>§</sup>Howard Hughes Medical Institute, University of California - Berkeley, Berkeley, California 94720, United States

<sup>‡</sup>Department of Chemistry and Biochemistry, University of California - Los Angeles, Los Angeles, California 90095, United States

## Supporting Information

**ABSTRACT:** The 1,3-dipolar cycloaddition of cyclooctynes with azides, also called “copper-free click chemistry”, is a bioorthogonal reaction with widespread applications in biological discovery. The kinetics of this reaction are of paramount importance for studies of dynamic processes, particularly in living subjects. Here we performed a systematic analysis of the effects of strain and electronics on the reactivity of cyclooctynes with azides through both experimental measurements and computational studies using a density functional theory (DFT) distortion/interaction transition state model. In particular, we focused on biarylazacyclooctynone (BARAC) because it reacts with azides faster than any other reported cyclooctyne and its modular synthesis facilitated rapid access to analogues. We found that substituents on BARAC’s aryl rings can alter the calculated transition state interaction energy of the cycloaddition through electronic effects or the calculated distortion energy through steric effects. Experimental data confirmed that electronic perturbation of BARAC’s aryl rings has a modest effect on reaction rate, whereas steric hindrance in the transition state can significantly retard the reaction. Drawing on these results, we analyzed the relationship between alkyne bond angles, which we determined using X-ray crystallography, and reactivity, quantified by experimental second-order rate constants, for a range of cyclooctynes. Our results suggest a correlation between decreased alkyne bond angle and increased cyclooctyne reactivity. Finally, we obtained structural and computational data that revealed the relationship between the conformation of BARAC’s central lactam and compound reactivity. Collectively, these results indicate that the distortion/interaction model combined with bond angle analysis will enable predictions of cyclooctyne reactivity and the rational design of new reagents for copper-free click chemistry.



## INTRODUCTION

Since its initial introduction as a bioorthogonal reaction, the strain-promoted 1,3-dipolar cycloaddition between cyclooctynes and azides (Figure 1a) has been utilized in a range of biological studies.<sup>1</sup> The reaction was developed in response to the dearth of tools available for the study of biomolecules in their native environments, and was designed to proceed rapidly and selectively *in vivo* without perturbing native biochemical functionality. Due to the strain activation inherent to cyclooctynes,<sup>2</sup> the reaction proceeds at a rate that is sufficient for *in vivo* labeling while avoiding the use of the toxic copper(I) catalysts traditionally employed in “click chemistry” with terminal alkynes.<sup>3,4</sup> As a result, the reaction between cyclooctynes and azides is often referred to as “copper-free click chemistry.”

In an effort to further enhance the utility of the strain-promoted reaction, several groups have contributed to a series of structurally varied cyclooctyne scaffolds that display differential reactivities toward the azide. A selection of these compounds is shown in b–d of Figure 1. All were designed on the basis of assuming that one can alter the reactivity of a cyclooctyne through modulation either of strain or electronics.

Cyclooctyne **1** (also called “Oct”, Figure 1b), the first cyclooctyne developed specifically as a bioorthogonal reagent, displays a second-order rate constant of  $2.4 \times 10^{-3} \text{ M}^{-1} \text{ s}^{-1}$  for the reaction with benzyl azide.<sup>5,6</sup> It was later shown that this rate can be enhanced through installation of fluorine atoms at the propargylic position. Monofluorinated cyclooctyne (MOFO, **2**) displays a second-order rate constant of  $4.3 \times 10^{-3} \text{ M}^{-1} \text{ s}^{-1}$ , whereas difluorinated cyclooctyne (DIFO, **3**) reacts with a rate constant of  $7.6 \times 10^{-2} \text{ M}^{-1} \text{ s}^{-1}$  (1.8-fold and 32-fold faster than Oct, respectively).<sup>3a,6</sup> The rate-enhancing effects of strain were subsequently demonstrated in the context of dibenzocyclooctyne (DIBO, **4**),<sup>7a,b</sup> dibenzoazacyclooctyne (DIBAC, **5**),<sup>7c</sup> and biarylazacyclooctynone (BARAC, **6**),<sup>7d</sup> which respectively react with azides 24-fold to 375-fold faster than is observed for Oct (Figure 1d).

The intention implicit in the design of compounds 4–6 was to increase strain by adding  $sp^2$  centers to the cyclooctyne ring. However, there may be more subtle consequences of these compounds’ structural modifications that actually oppose the

Received: January 4, 2012

Published: May 3, 2012

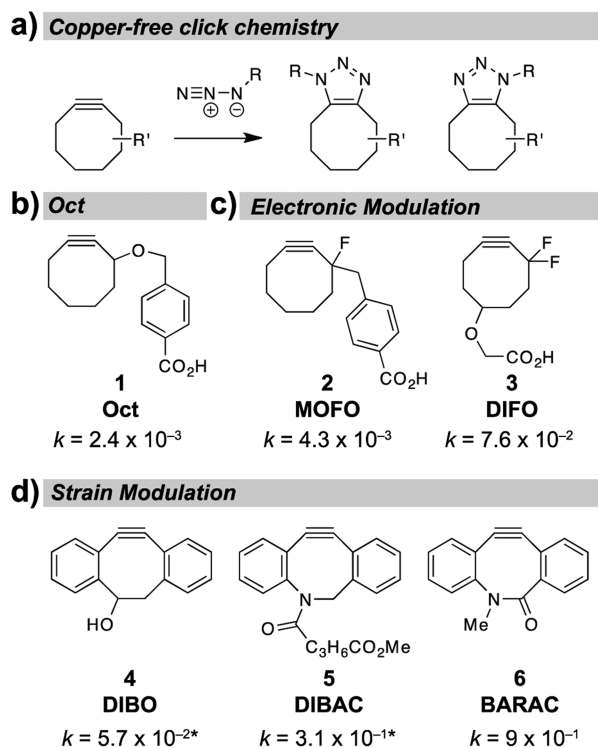


**Figure 1.** Reagent development for copper-free click chemistry. (a) The 1,3-dipolar cycloaddition between azides and cyclooctynes. (b) Oct, the first cyclooctyne developed as a bioorthogonal reagent, and its corresponding second-order rate constant for the reaction with benzyl azide.<sup>5,6</sup> The reactivity of a cyclooctyne can be altered through (c) electronic<sup>6,3a</sup> and (d) strain modulation.<sup>7</sup> All rate constants are second order ( $M^{-1} s^{-1}$ ) and were measured at room temperature in  $CD_3CN$  except for values noted with an asterisk (\*) which were measured in  $CD_3OD$ .

desired reactivity outcome. For example, while aryl ring fusion may enhance strain, the “flagpole” hydrogen atoms ortho to the aryl/cyclooctyne ring junction were predicted by Goddard and co-workers to decrease reactivity by steric interference with the azide in the transition state.<sup>8a</sup> The experimentally observed reactivity of biaryl cyclooctynes likely reflects a balance of these rate-enhancing and -diminishing effects. This example underscores the difficulty inherent to rational design of new cyclooctynes with tailored kinetic properties. Many structural perturbations affect more than one contributor to reactivity, e.g., strain, sterics, and electronics. Without a better understanding of their relative influence on transition state activation energies, these parameters cannot be readily optimized to achieve a desired outcome. In principle, one might derive a set of rules that links structure and reactivity solely on the basis of empirical data. However, cyclooctynes are generally challenging synthetic targets that do not lend themselves to extensive analoging.

In previous work, density functional theory (DFT) models have been employed to analyze reactions of cyclooctynes with azides and have proven to be useful predictors of relative transition state activation energies.<sup>8</sup> Here we performed a systematic analysis of the effects of strain and electronics on the reactivity of cyclooctynes with azides, using both empirical data and a DFT-based distortion/interaction transition state model.<sup>8b,c</sup> We focused our analysis on a series of differentially substituted BARAC analogues, comparing their second-order rate constants in the cycloaddition reaction with benzyl azide to

those predicted by DFT calculations. We also investigated the relationship between alkyne bond angles and reactivity and determined the conformation of BARAC’s central lactam, which has significant energetic consequences. The results herein provide a framework for understanding and predicting cycloaddition kinetics.

## ■ DISTORTION/INTERACTION MODEL

The distortion/interaction model deconstructs the activation energy of a reaction into two components: the distortion energy, which is dependent on ground state strain, and the interaction energy, which is governed by transition state electronics.<sup>8b,c</sup> In this model, the transition state energy ( $\Delta E^\ddagger$ ) of a reaction is defined as the sum of distortion energy ( $\Delta E_d^\ddagger$ ), the energy required to distort the alkyne and azide into their preferred transition state conformations, and interaction energy ( $\Delta E_i^\ddagger$ ), the energy lowering upon favorable orbital overlap between the azide and the alkyne ( $\Delta E^\ddagger = \Delta E_d^\ddagger + \Delta E_i^\ddagger$ ). Thus, the activation energy of a reaction can be altered by changing either the distortion energy or the interaction energy required to reach the transition state.

In the case of the 1,3-dipolar cycloaddition of 2-butyne with methyl azide (Figure 2a), our calculations indicate that 29.9 kcal/mol energy is required to distort the ground state substrates into their preferred transition state conformations. Upon distortion, the alkyne and azide interact, lowering the energy of the overall system by  $-9.0$  kcal/mol through a favorable orbital overlap that can only be achieved via the geometry of the distorted state. Combining the effects of distortion and interaction, we calculate an overall transition state activation energy of 20.9 kcal/mol ( $\Delta E^\ddagger = \Delta E_d^\ddagger + \Delta E_i^\ddagger$ ). In reality, distortion and interaction are not independent processes but instead occur simultaneously to bring reactants directly to their transition state geometries. However, this model breaks up activation energy into two imaginary distortion and interaction processes to allow a more detailed analysis of reaction strain and electronics.

An example of how electronic perturbation can affect interaction and distortion energies is illustrated by comparing the above reaction coordinate to that for the reaction of 1,1,1,4,4,4-hexafluoro-2-butyne with methyl azide (Figure 2b). In this case, the interaction energy is more negative than that calculated for 2-butyne ( $\Delta E_{i,\text{hexafluoroalkyne}}^\ddagger = -12.2$  kcal/mol vs  $\Delta E_{i,2\text{-butyne}}^\ddagger = -9.0$  kcal/mol). This change results from electronic perturbation of the alkyne LUMO energy via mixing of the alkyne  $\pi$ -system with  $\sigma_{C-F}^*$ . Alabugin and co-workers have shown that the observed acceleration results from hyperconjugative stabilization of the cycloaddition transition state via electron donation from the in-plane alkyne  $\pi$ -orbital to the  $\sigma_{C-F}^*$ -orbital.<sup>9</sup>

As both 1,1,1,4,4,4-hexafluoro-2-butyne and 2-butyne are relatively unstrained molecules, we would expect their distortion energies to be similar for the reaction with methyl azide. However, calculations indicate a larger total distortion energy for the reaction of 2-butyne by 5.3 kcal/mol ( $\Delta E_{d,\text{total},2\text{-butyne}}^\ddagger = 29.9$  kcal/mol and  $\Delta E_{d,\text{total},\text{hexafluoroalkyne}}^\ddagger = 24.6$  kcal/mol). The data in a and b of Figure 2 indicate that this difference results both from a change in alkyne transition state distortion energy upon perfluorination as well as from a decrease in azide distortion energy. That both the alkyne and azide undergo shifts in distortion energy in the perfluorinated case indicates that the transition state occurs at an earlier point on the reaction coordinate. Calculated azide bond angles

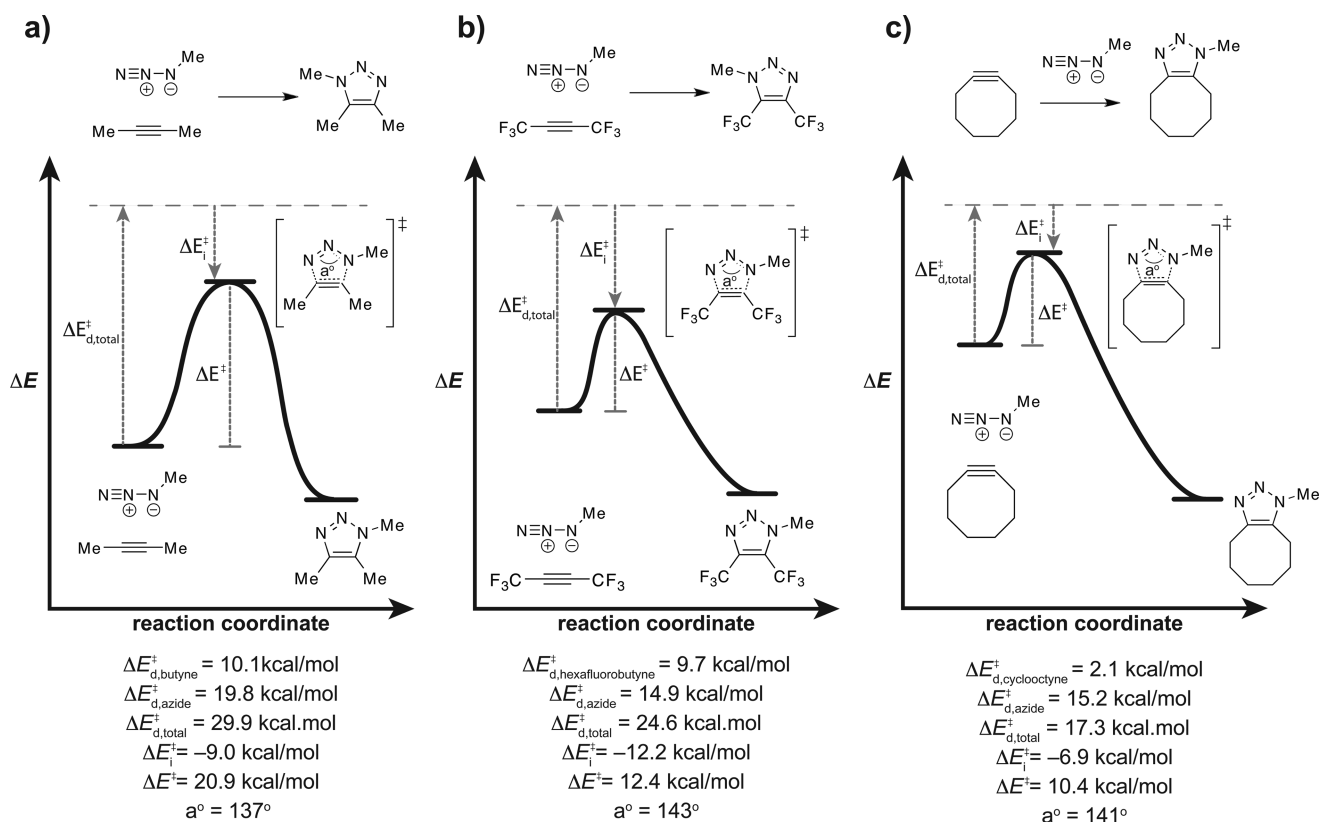


**Figure 2.** Distortion/interaction model. (a) Activation energy ( $\Delta E^{\ddagger}$ ) for the reaction between 2-butyne and methyl azide is the sum of distortion energy ( $\Delta E_{d,i}^{\ddagger}$ ) and interaction energy ( $\Delta E_i^{\ddagger}$ ). (b) Perfluorination of the alkyne reduces  $\Delta E^{\ddagger}$  of the reaction by increasing the magnitude of stabilizing interactions in the transition state and decreasing distortion energy. (c) Constraining the alkyne into an eight-membered ring reduces  $\Delta E^{\ddagger}$  by decreasing the distortion energy required to bend the starting materials into their preferred transition state conformations. For a–c, calculated values are electronic energies, the potential energy of the molecule on a vibrationless potential energy surface. As all reactions are represented on separate energy diagrams, the depictions are only intended to facilitate comparisons of  $\Delta E^{\ddagger}$ ,  $\Delta E_{d,i}^{\ddagger}$ , and  $\Delta E_i^{\ddagger}$  values and not the overall energies of starting materials or triazole products. Calculations were performed using B3LYP/6-31G(d). See Supporting Information for details.

provide further evidence for an early transition state upon perfluorination. Whereas the azide is bent to  $137^{\circ}$  in the transition state of the 2-butyne reaction, it is only bent to  $143^{\circ}$  in the transition state of the perfluorinated-alkyne reaction (Figure 2). Thus, the effect of propargylic fluorination is 2-fold when considering the distortion/interaction model; the fluorine atoms enhance transition state interaction energies, which facilitates an early transition state where less distortion is required for both reactants.

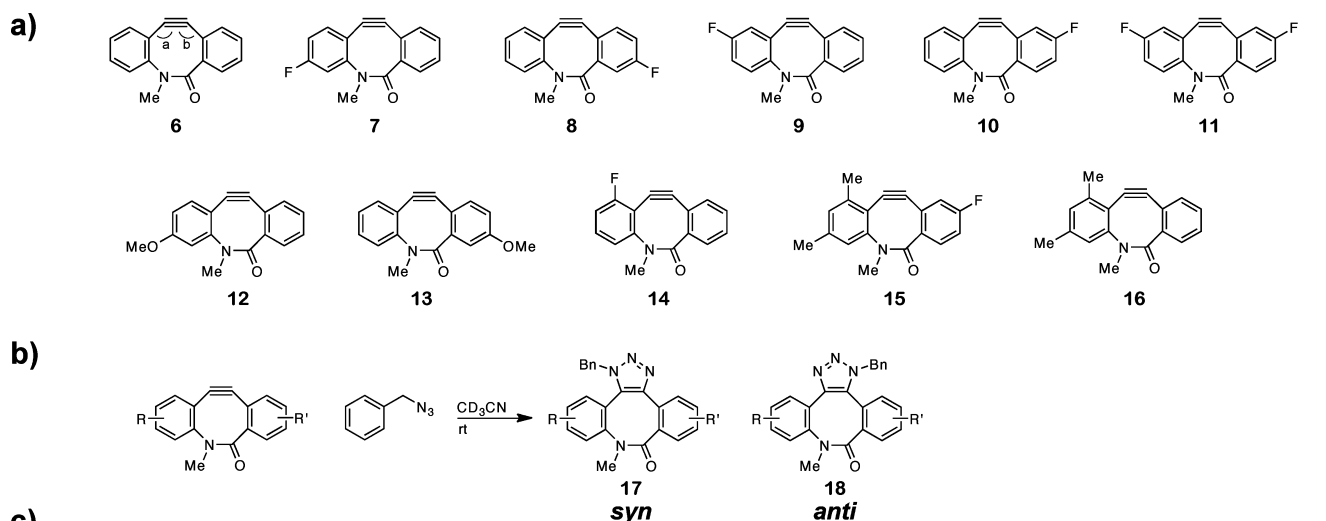
The effects of distortion energy modulation in the context of the cyclooctyne have previously been discussed<sup>8b,c</sup> and are summarized in Figure 2c. The alkyne bond angles in cyclooctyne are bent from linearity, and the molecule is therefore destabilized relative to a linear isomer. Because it is already distorted toward the transition state geometry, the cyclooctyne requires less distortion energy to reach its preferred transition state geometry than does a linear alkyne ( $\Delta E_{d,2\text{-butyne}}^{\ddagger} = 10.1 \text{ kcal/mol}$  and  $\Delta E_{d,\text{cyclooctyne}}^{\ddagger} = 2.1 \text{ kcal/mol}$ ). In addition, calculations show that the distortion energy of methyl azide is lower for the reaction with cyclooctyne than it is for the reaction with 2-butyne. We again attribute this difference to the position of the transition state along the reaction coordinate; here, ground state destabilization of the strained cyclooctyne generates an early transition state, thereby reducing the distortion required for the azide to reach its transition state geometry. This shift in the position of the transition state in response to the greater exothermicity of the

strained alkyne reaction is also consistent with the Hammond Postulate. As a result of this significant reduction in distortion energy, cyclooctyne displays a lower overall activation energy for the cycloaddition reaction than does 2-butyne. In this way, strain (i.e., distortion) promotes the cycloaddition.

Because this model is capable of distinguishing the effects of strain and electronics on transition state energies, we chose to apply it to the study of cyclooctyne reactivity. We began by preparing a series of substituted BARAC analogues and analyzing their reactivities experimentally and computationally.

## ■ REACTIVITY OF BARAC AND ANALOGUES

The modular nature of BARAC's synthesis<sup>7d</sup> rendered this scaffold amenable to derivatization with aryl ring substituents. Previous analyses of the difluorinated cyclooctyne DIFO (3, Figure 1c) suggested that addition of fluorine atoms at the propargylic position enhances reaction rates by increasing interaction energies and decreasing distortion energies in the transition state.<sup>8b,c</sup> We were curious as to whether comparable interaction energy changes might be affected through installation of fluorine atoms on BARAC's aryl rings, and, alternatively, whether electron-donating methoxy groups would affect reaction kinetics in an opposite manner. As well, we sought to analyze the steric effects of flagpole methyl substituents on the rate of the reaction. Accordingly, compounds 7–16 (Figure 3a) were selected as the targets for our study. Compounds 7–10 possess a single fluorine atom



Compound	angle a (°)	angle b (°)	$k_{\text{exp}}(\text{M}^{-1} \text{s}^{-1})$	$\Delta G_{\text{exp}}^{\ddagger}$ (kcal/mol)	$\Delta E_{\text{d,calc}}^{\ddagger}$ (kcal/mol)	$\Delta E_{\text{i,calc}}^{\ddagger}$ (kcal/mol)	$\Delta E_{\text{calc}}^{\ddagger}$ (kcal/mol)	$\Delta G_{\text{calc}}^{\ddagger}$ (kcal/mol)
6	152.7 (153)	153.0 (153)	$0.9 \pm 0.1$	17.5	syn = 16.5 anti = 16.7	syn = -8.2 anti = -8.8	syn = 8.3 anti = 8.0	syn = 24.0 anti = 24.1
7	152.4	153.1	$1.1 \pm 0.1$	17.4	syn = 16.6 anti = 16.6	syn = -8.3 anti = -8.9	syn = 8.2 anti = 7.7	syn = 24.1 anti = 24.0
8	153.0	152.7	$1.10 \pm 0.04$	17.4	syn = 16.4 anti = 16.8	syn = -8.4 anti = -8.9	syn = 8.0 anti = 7.9	syn = 23.8 anti = 24.0
9	152.3	153.4	$1.0 \pm 0.1$	17.4	syn = 16.6 anti = 16.7	syn = -8.6 anti = -9.0	syn = 8.0 anti = 7.7	syn = 23.7 anti = 23.7
10	153.0	152.7	$1.2 \pm 0.1$	17.3	syn = 16.4 anti = 16.8	syn = -8.4 anti = -9.0	syn = 8.0 anti = 7.8	syn = 23.7 anti = 23.9
11	152.5	153.1	$1.6 \pm 0.1$	17.1	syn = 16.4 anti = 16.7	syn = -8.7 anti = -9.2	syn = 7.7 anti = 7.5	syn = 23.5 anti = 23.6
12	152.6	152.8	$1.0 \pm 0.1$	17.4	syn = 16.2 anti = 16.5	syn = -8.2 anti = -8.7	syn = 8.1 anti = 7.9	syn = 23.9 anti = 24.0
13	152.5 (154)	153.0 (153)	$1.1 \pm 0.1$	17.4	syn = 16.4 anti = 16.6	syn = -8.1 anti = -8.7	syn = 8.3 anti = 8.0	syn = 23.8 anti = 23.9
14	151.1	153.7	$0.058 \pm 0.003$	19.1	syn = 17.3 anti = 19.4	syn = -8.2 anti = -8.3	syn = 9.1 anti = 11.1	syn = 24.7 anti = 26.0
15	153.6 (155)	152.1 (152)	$0.0019 \pm 0.0003^{**}$	21.1	syn = 19.6 anti = 21.7	syn = -7.9 anti = -8.2	syn = 11.7 anti = 13.4	syn = 28.2 anti = 30.1
16	153.0 (154)	152.7 (152)	$0.0009 \pm 0.0001^{**}$	21.5	syn = 19.7 anti = 21.6	syn = -7.7 anti = -8.0	syn = 12.0 anti = 13.6	syn = 28.3 anti = 30.2

**Figure 3.** Bond angles and reactivities of BARAC analogues. (a) BARAC analogues targeted for our initial study of distortion/interaction modulation. (b) Reactivity was probed empirically by measuring the second-order rate constant for the reaction of each analogue with benzyl azide in  $\text{CD}_3\text{CN}$  at rt by  $^1\text{H}$  NMR spectroscopy. (c) Table shows both calculated and measured (X-ray crystallography data shown in parentheses) alkyne bond angles for compounds 6–16 as well as measured second-order rate constants and activation free energies ( $\Delta G_{\text{exp}}^{\ddagger}$ ) for the model reaction with benzyl azide. Also shown are calculated interaction ( $\Delta E_{\text{i,calc}}^{\ddagger}$ ) and total distortion energies ( $\Delta E_{\text{d,calc}}^{\ddagger} = \Delta E_{\text{d,calc,azide}}^{\ddagger} + \Delta E_{\text{d,calc,alkyne}}^{\ddagger}$ ) as well as overall electronic energies of activation ( $\Delta E_{\text{calc}}^{\ddagger}$ ) and free energies of activation ( $\Delta G_{\text{calc}}^{\ddagger}$ ) for the reaction of each analogue with methyl azide. All computational data provided for compounds 6–16 are for the *trans*-BARAC isomer. \*Free energies were calculated for the reaction in acetonitrile. \*\*The second-order rate constants shown for 15 and 16 were measured in  $\text{CDCl}_3$  due to the limited solubility of 15 in  $\text{CD}_3\text{CN}$ .

variously positioned around BARAC's two aryl rings. Compound 11 is doubly fluorinated. On the other end of the spectrum, compounds 12 and 13 have single methoxy groups on the aryl rings. Compound 14 is monofluorinated at the flagpole position, potentially generating steric hindrance in the transition state. Finally, compounds 15 and 16 possess methyl substituents at the flagpole position. All analogues were

synthesized according to the route published by Jewett et al.<sup>7d</sup> Details are provided in the Supporting Information (SI).

As a platform for computational studies, we first analyzed the bond angles and conformation of the parent compound BARAC using X-ray crystallography and DFT calculations. Figure 4a shows DFT geometry optimizations performed with B3LYP and the 6-31G(d) basis set. The results indicate that the *trans* conformation of the central amide bond is preferred to the

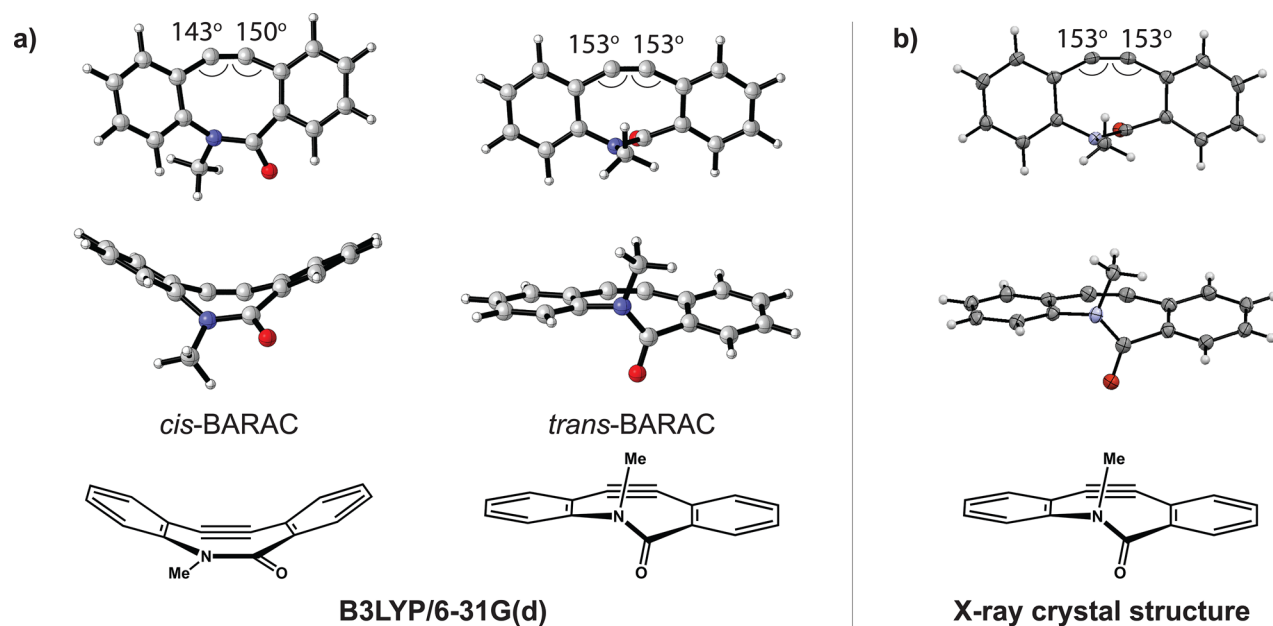


**Figure 4.** Structural analysis of BARAC. (a) DFT calculations (B3LYP/6-31G(d)) of *cis*- and *trans*-BARAC. (b) Front and side view of BARAC obtained via X-ray crystallography. Crystalline BARAC exists as the *trans* conformer. Thermal ellipsoid plots are shown at 50% probability.

*cis* conformation by  $\Delta\Delta G_{\text{solv}} = 9.4$  kcal/mol in acetonitrile. X-ray data support this model, indicating that in crystal form, BARAC preferentially occupies the *trans* conformation (Figure 4b).

Interestingly, DFT calculations show that the conformation of the amide functionality dramatically influences BARAC's alkyne bond angles. As shown in Figure 4a, both alkyne angles in *trans*-BARAC are 153°, whereas in *cis*-BARAC the angles are compressed to 143° and 150°. These results suggest that *cis*-BARAC is higher in energy than *trans*-BARAC due to increased alkyne distortion and also imply that *cis*-BARAC would display enhanced reactivity relative to that of *trans*-BARAC in the cycloaddition reaction with azides. DFT calculations of free energies of activation in acetonitrile ( $\Delta G_{\text{solv}}^{\ddagger}$ ) for this reaction support our hypothesis. *trans*-BARAC has a  $\Delta G_{\text{solv}}^{\ddagger}$  of 24.0 kcal/mol, whereas *cis*-BARAC has a  $\Delta G_{\text{solv}}^{\ddagger}$  of 18.0 kcal/mol.

We performed energy optimization calculations on substituted BARAC analogues 7–16 as well, and the results also indicated that the *trans* conformation is preferred to the *cis* conformation by  $\Delta\Delta G_{\text{solv}} = 9.1$ –9.7 kcal/mol (SI). We then calculated  $\Delta G_{\text{solv}}^{\ddagger}$  values for the reactions of compounds 7–16 with methyl azide, and results indicate that for compounds 7–13, reaction of the *trans*-conformer is a lower-energy process by 3.0–4.5 kcal/mol than is isomerization to the *cis*-conformer followed by reaction to form the triazole. These results suggest that compounds 7–13 react predominantly as the *trans* conformer. Thus, we focus the remainder of the calculations in this section on *trans*-BARAC. As discussed later,  $\Delta G_{\text{solv}}^{\ddagger}$ 's for reactions of the *cis*- and *trans*-conformers are similar in energy for compounds 14–16, suggesting a Curtin-Hammett controlled reaction.

The table shown in Figure 3c shows the results of DFT calculations of alkyne bond angles as well as empirical bond angle measurements obtained by X-ray crystallography (shown in parentheses) for select compounds in the *trans* conformation. We conclude from these data that aryl substitution does

not impose significant structural changes, as all compounds exhibit alkyne bond angles close to 153°.

We next measured the second-order rate constants of the reactions of 6–16 with benzyl azide (Figure 3b). Compounds 6–10 and 12–13 exhibited rate constants that do not lie outside the range of experimental error.<sup>10,11</sup> Compound 11, however, showed a roughly 75% increase in reactivity relative to that of 6 ( $k_{11} = 1.6 \pm 0.1 \text{ M}^{-1} \text{ s}^{-1}$  versus  $k_6 = 0.9 \pm 0.1 \text{ M}^{-1} \text{ s}^{-1}$ ). Given the similar reactivities of 6–10, 12, and 13, we expected these compounds to display transition state distortion and interaction energies of similar magnitude. DFT calculations were used to model the reaction of each analogue with methyl azide, as calculations show that methyl azide behaves similarly to benzyl azide for the reaction with 6 (data provided in the SI). In discussing the results of these calculations, we define triazole 17 (Figure 3b) as the *syn*-regioisomer and triazole 18 (Figure 3b) as the *anti*-regioisomer.

Computational data indicate that compounds 6–10, 12 and 13 do in fact exhibit similar energetics in their transition states, with distortion energies for all seven compounds lying between 16.2 and 16.6 kcal/mol for the *syn*-regioisomer and between 16.5 and 16.8 kcal/mol for the *anti*-regioisomer. These data are consistent with our observations that the compounds have nearly identical alkyne bond angles (additional structural data are provided in the SI). Similarly, calculated interaction energies were alike for these compounds with values between –8.1 and –8.6 kcal/mol for the *syn*-regioisomer and between –8.7 and –9.0 kcal/mol for the *anti*-regioisomer. As a result, overall energies of activation ( $\Delta E^{\ddagger} = \Delta E_{\text{d}}^{\ddagger} + \Delta E_{\text{i}}^{\ddagger}$ ) for these compounds are quite comparable, falling within the range of 8.0–8.3 kcal/mol for the *syn*-regioisomer and between 7.7–8.0 kcal/mol for the *anti*-regioisomer.

Calculated free energies of activation in acetonitrile ( $\Delta G_{\text{calc}}^{\ddagger}$ ) are also similar for compounds 6–10, 12 and 13. For both the *syn*- and *anti*-regioisomers,  $\Delta G_{\text{calc}}^{\ddagger}$  lies between 23.7 and 24.1 kcal/mol. These calculations systematically overestimate the

true free energies of activation by about 6.5 kcal/mol. This error has been previously noted in applications of B3LYP to cycloaddition reactions.<sup>12,13</sup> Such calculations also overestimate the entropic penalty associated with the transition states of bimolecular reactions.

Compound **11** was the only analogue with substantially increased reactivity compared to BARAC, and accordingly, its transition state interaction energies ( $\Delta E_{i,\text{calc}}^\ddagger$  values of  $-8.7$  kcal/mol (*syn*) and  $-9.2$  kcal/mol (*anti*)) were the largest measured in this study. Interestingly, we found that the transition state distortion energies for this analogue lie within the range of those calculated for the other compounds ( $\Delta E_{d,\text{calc}}^\ddagger = 16.4$  kcal/mol (*syn*) and  $\Delta E_{d,\text{calc}}^\ddagger = 16.7$  kcal/mol (*anti*)). As a result, combined activation energies for compound **11** are lower than those observed for the other analogues ( $\Delta E_{\text{calc}}^\ddagger = 7.7$  kcal/mol (*syn*) and  $\Delta E_{\text{calc}}^\ddagger = 7.5$  kcal/mol (*anti*)). The calculated free energies of activation in acetonitrile ( $\Delta G_{\text{calc}}^\ddagger$ ) for compound **11** follow a similar trend (Figure 3c). These data indicate that the enhanced reaction rate observed for **11** is a result of electronic modulation that generates enhanced stabilizing interactions in the transition state. Modulation of strain and distortion energy does not appear to play a significant role in the rate enhancement.

Our experimental results also provide insight into the effects of sterics on cyclooctyne reactivity. We were surprised to find that compounds **14–16**, which all contain a flagpole substituent ortho to the alkyne, exhibit dramatic decreases in their rates relative to the parent BARAC ( $k_{14} = 5.8 \pm 0.3 \times 10^{-2} \text{ M}^{-1} \text{ s}^{-1}$  in  $\text{CD}_3\text{CN}$ ,  $k_{15} = 1.9 \pm 0.3 \times 10^{-3} \text{ M}^{-1} \text{ s}^{-1}$  in  $\text{CDCl}_3$ , and  $k_{16} = 9 \pm 1 \times 10^{-4} \text{ M}^{-1} \text{ s}^{-1}$  in  $\text{CDCl}_3$ ). Calculations show that these three compounds display corresponding increases in transition state distortion energies relative to analogues **6–13**. This enhanced distortion is due to the close proximity of the substituent to the alkyne and its orientation directly toward the path of the incoming azide, requiring both the azide and the alkyne to distort to a higher degree in the transition state. Figure 5 gives both a front and side view of the transition state of the reaction of compounds **6** and **15** with methyl azide, and it is clear that the methyl group is causing unfavorable steric interactions. Even a relatively small fluorine atom in this position, as in compound **14**, causes a significant increase in transition state distortion energy (Figure 3c). By contrast, the transition state interaction energies of compounds **14–16** are similar to those of the other BARAC analogues. As a result, **14–16** have higher activation barriers than do the other analogues tested, resulting in the observed orders of magnitude decrease in reactivity.

Overall, our analyses of compounds **6–16** indicate that aryl substitution can affect minor reactivity changes by altering transition state interaction energies (e.g., compound **11**) and substantial rate changes by increasing steric hindrance in the transition state (e.g., compounds **14–16**). For compounds **6–13**, we did not observe any changes in reactivity due to modulation of transition state distortion energies, and we hypothesize that the enhanced distortion energies observed for **14–16** are a result of sterics rather than alkyne strain.

## ■ ALKYNE BOND ANGLES AS A MEASURE OF REACTIVITY

Compounds **6–13**, which share similar reactivities and transition state distortion energies, also possess similar structures with alkyne bond angles close to  $153^\circ$  (Figure 3c). This observation led us to hypothesize that alkyne bond angles

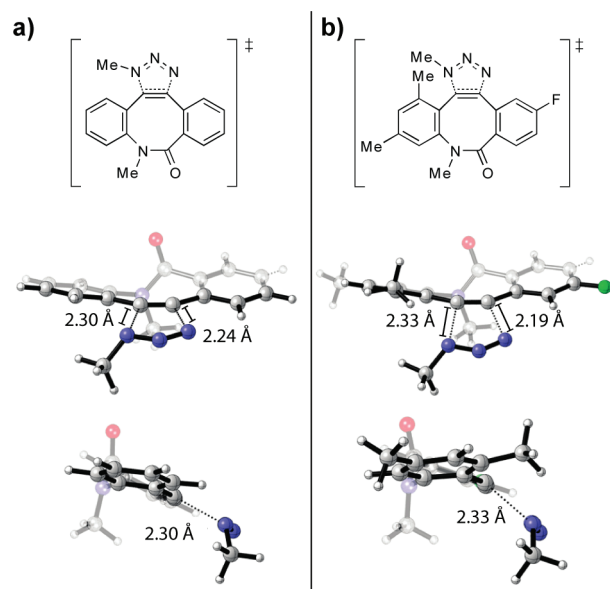


**Figure 5.** Flagpole methyl substituents sterically hinder the transition state. (a) Front and side views of the transition state of the reaction of **6** with methyl azide. (b) Front and side views of the transition state of the reaction of **15** with methyl azide. Transition states were modeled using B3LYP/6-31G(d).

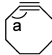
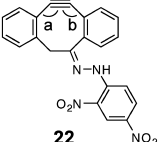
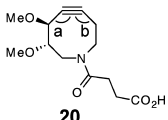
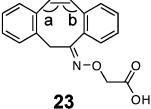
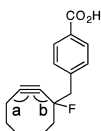
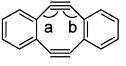
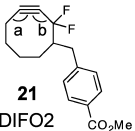
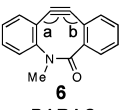
may correlate with transition state activation energies for the cycloaddition with organic azides. If so, one may be able to predict the reactivity of a given cyclooctyne by determining its alkyne bond angles either through X-ray crystallography or DFT geometry optimizations.

Table 1 shows compiled X-ray structural data for a series of cyclooctynes as well as second-order rate constants for the reaction of each compound with benzyl azide (complete crystallographic data sets for compounds **2**, **6**, **20**, and **21** are in the SI; crystallographic or electron diffraction data for the other compounds are referenced in Table 1). Although kinetic parameters for the reaction of cyclooctyne itself (**19**) with organic azides have not been reported, we include the average bond angle of cyclooctyne<sup>14</sup> in Table 1 as a point of comparison.

The data in Table 1 indicate a general correlation between alkyne bond angle distortion and cyclooctyne reactivity. Dimethoxyazacyclooctyne (DIMAC,<sup>15</sup> **20**) exhibits bond angles of  $158^\circ$  and  $157^\circ$ , structural deviations of only  $1^\circ$  and  $2^\circ$ , respectively, from the parent cyclooctyne **19**. Thus, neither DIMAC's endocyclic nitrogen nor its exocyclic substituents distort the alkyne bond angles to a significant extent. Installation of a fluorine atom at the propargylic position in MOFO<sup>6</sup> (**2**) slightly enhances alkyne distortion at angle b through a bond polarization mechanism that has been extensively documented in substituted arynes.<sup>16</sup> Angle b in MOFO is  $4^\circ$  more distorted than the average bond angle in cyclooctyne ( $155^\circ$  versus  $159^\circ$ , respectively). Conversely, angle a is less distorted in MOFO ( $160^\circ$  versus  $159^\circ$ ). Overall, the structural differences between MOFO and DIMAC are small, and, correspondingly only minor reactivity differences between the two are observed ( $k_{\text{MOFO}} = 4.3 \times 10^{-3} \text{ M}^{-1} \text{ s}^{-1}$  and  $k_{\text{DIMAC}} = 3.0 \times 10^{-3} \text{ M}^{-1} \text{ s}^{-1}$ ).<sup>6,15</sup>

As previously mentioned, installation of an additional fluorine atom at the propargylic position as in DIFO<sup>17</sup> (**21**) further enhances alkyne distortion at angle b ( $151^\circ$ ) through

Table 1. Reactivity and Alkyne Bond Angles<sup>a</sup>

cyclooctyne	a (°)	b (°)	rate constant (M <sup>-1</sup> s <sup>-1</sup> )	ref.	cyclooctyne	a (°)	b (°)	rate constant (M <sup>-1</sup> s <sup>-1</sup> )	ref.
 <b>19</b> cyclooctyne	159	N/A	N/A	14	 <b>22</b>	152	157	N/A	18
 <b>20</b> DIMAC	158	157	3.0 x 10 <sup>-3</sup>	15, SI	 <b>23</b>	N/A	N/A	6.1 x 10 <sup>-2***</sup>	7b
 <b>2</b> MOFO	160	155	4.3 x 10 <sup>-3</sup>	6, SI	 <b>24</b>	156	155	6.3 x 10 <sup>-2***</sup>	14, 19
 <b>21</b> DIFO2	162	151	4.2 x 10 <sup>-2*</sup>	17, SI	 <b>6</b> BARAC	153	153	9 x 10 <sup>-1</sup>	7d, SI

<sup>a</sup>Cyclooctyne bond angles and second-order rate constants for the reaction with benzyl azide in acetonitrile at rt. All bond angles were measured via X-ray crystallography with the exception of compound **19**, which was analyzed by electron diffraction in the gas phase. All data are referenced in the table, and details of the measurements first reported in this publication are located in the SI. N/A = data not available. \*Rate was measured for the acid form of DIFO2. \*\*Rate constant measured in methanol.

bond polarization. This additional bending at angle b is accompanied by a reduction in distortion at angle a (162° for DIFO2 vs 160° for MOFO). Despite strain reduction at angle a, however, the data suggest that the highly distorted nature of angle b in DIFO2 may contribute to the order of magnitude rate enhancement observed for this compound relative to that for MOFO ( $k_{\text{DIFO2}} = 4.2 \times 10^{-2} \text{ M}^{-1} \text{ s}^{-1}$  versus  $k_{\text{MOFO}} = 4.3 \times 10^{-3} \text{ M}^{-1} \text{ s}^{-1}$ ).<sup>6,17</sup>

The structure/reactivity trend observed for DIMAC, MOFO, and DIFO2 is also evident in the biaryl cyclooctyne series. Dibenzocyclooctyne **22**, reported by Kornmayer et al., exhibits bond angles of 152° and 157° and therefore is only slightly less distorted than DIFO2 at one angle but significantly more distorted than DIFO2 at the other.<sup>18</sup> Although rate data are not available for this particular compound, a related oxime-substituted dibenzocyclooctyne (**23**) has been reported by Boons and co-workers to display a second-order rate constant of  $k = 6.1 \times 10^{-2} \text{ M}^{-1} \text{ s}^{-1}$  for the reaction with benzyl azide in methanol.<sup>7b</sup> The enhanced alkyne distortion observed at both alkyne angles in compound **22** (vs just one alkyne bond angle in DIFO2) may contribute to its heightened reactivity. Dibenzocyclooctadiyne **24**, with alkyne bond angles of 156° and 155°,<sup>14,19</sup> seems to distribute alkyne distortion more symmetrically across the bond but overall is not significantly more distorted than **23**. The reaction of compound **24** with benzyl azide was reported by Kii et al. to proceed with a second-order rate constant of  $k = 6.3 \times 10^{-2} \text{ M}^{-1} \text{ s}^{-1}$ .<sup>19b</sup> As

expected given their similar degrees of overall alkyne distortion, the reactivity of compound **24** is similar in magnitude to that measured for compound **23** ( $k = 6.1 \times 10^{-2} \text{ M}^{-1} \text{ s}^{-1}$ ).

Relative to compounds **23** and **24**, BARAC (**6**) is significantly more distorted. With both alkyne bond angles at 153°, BARAC's structure exhibits the greatest overall deviation from cyclooctyne (159°). Accordingly, BARAC exhibits a second-order rate constant that is an order of magnitude greater than that of compound **24** ( $k_{\text{BARAC}} = 9 \times 10^{-1} \text{ M}^{-1} \text{ s}^{-1}$  vs  $k_{24} = 6.3 \times 10^{-2} \text{ M}^{-1} \text{ s}^{-1}$ ).<sup>19b</sup> In summary, compounds **6** and **22–24** follow the same distortion/reactivity trend observed for DIMAC, MOFO, and DIFO2, with increased overall alkyne bond angle distortion correlating with increased reactivity.

## ■ EFFECTS OF BARAC'S AMIDE BOND STRUCTURE ON REACTIVITY AND REGIOSELECTIVITY

The extreme distortion of BARAC's alkyne bond angles compared to that of bond angles of other dibenzocyclooctynes may reflect adjustments of the cyclooctyne ring geometry to accommodate the lactam functionality. We speculate that BARAC's endocyclic amide bond enhances the overall ring strain of the compound by contributing some partial double bond character to the position directly opposite the alkyne. Semi-empirical calculations by Meier et al. predict that the fully unsaturated cyclooctyne **25** (Figure 6a) would possess almost 3-fold more ring strain than the parent cyclooctyne **19**.<sup>2b</sup> A

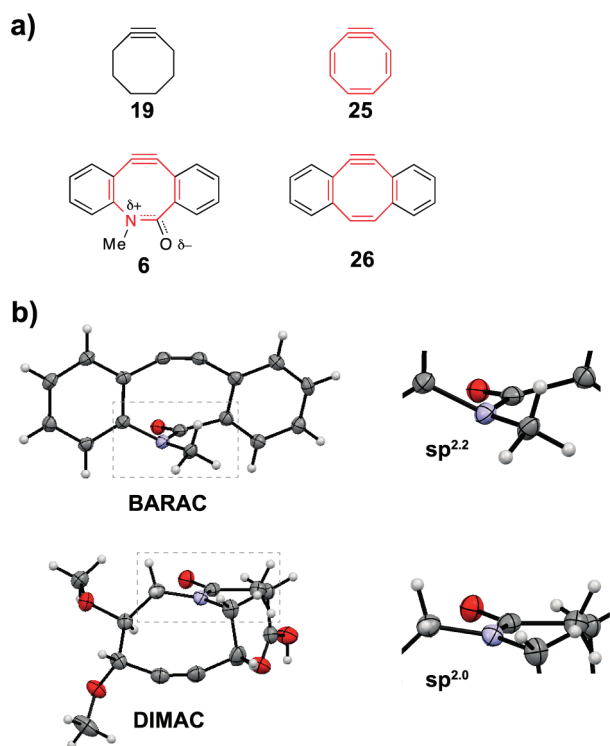


**Figure 6.** Strain modulation through rehybridization. (a) Ring strain in cyclooctynes increases with increased unsaturation. We hypothesize that BARAC's fused aryl rings and central lactam contribute significantly to the compound's ring strain. (b) X-ray crystal structures show that the nitrogen atom of BARAC's central lactam is  $sp^{2.2}$  hybridized, whereas DIMAC's amide nitrogen atom is  $sp^{2.0}$  hybridized. Thermal ellipsoid plots are shown at 50% probability.

related dibenzocyclooctenyne (**26**, Figure 6a) has been synthesized but is not bench-stable,<sup>14</sup> consistent with the notion that ring strain increases with cyclooctyne unsaturation. BARAC shares structural features with compounds **25** and **26** but is relatively stable, prompting us to investigate the properties of BARAC's central amide bond.

An interesting comparison can be made between the hybridization indices of the nitrogen atoms in BARAC's and DIMAC's (**20**, Table 1) amide bonds, which we calculated using the sum of the bond angles surrounding the atom.<sup>20</sup> Whereas the amide nitrogen of DIMAC displays the expected  $sp^2$  hybridization, that of BARAC is slightly pyramidalized with an  $sp^{2.2}$  hybridization index. Though deviation from  $sp^2$  hybridization in amides is generally thermodynamically disfavored, such distortion may reduce BARAC's overall ring strain by diminishing the double bond character and planarity of the lactam. This structural flexibility allows BARAC to balance reactivity and stability through amide nitrogen rehybridization.

Another notable feature of BARAC's amide bond is that its conformational state appears to impact regioselectivity in the alkyne-azide cycloaddition reaction. Whereas parent compound **6** reacts with benzyl azide to give a 1:1 mixture of *syn*- and *anti*-triazole products, analogues **15** and **16** generate *syn*/*anti*-triazole product ratios of 3:1 and 2:1, respectively, wherein the favored product reflects the more sterically hindered transition state. Though counterintuitive on its face, this observation follows the general trend predicted using the distortion/interaction model.<sup>21</sup> However, the magnitude of the regioisomeric preference is strongly affected by the conformation of BARAC's lactam in the ground state. For both **15** and **16**, our calculations predict a 25:1 preference for the *syn*-regioisomer when BARAC reacts through its lowest-energy *trans*-conformer, but when the calculation was performed using *cis*-BARAC as a substrate, the predicted product ratio was 1.2:1 *syn/anti* for **15** and 0.8:1 *syn/anti* for **16**. Our experimentally observed product ratio may therefore reflect the presence of both conformers in solution, which, if interconvertible, would generate a Curtin-Hammett-controlled product distribution.

We calculated the barrier to amide bond isomerization for BARAC (**6**) and analogues **15** and **16** (a and b of Figure 7). For BARAC, the barrier to *cis/trans* isomerization is 15.9 kcal/mol. With the energy of *trans*-BARAC set to 0 kcal/mol, reaction of the *trans*-conformer with methyl azide has an energetic barrier of 24.0 or 24.1 kcal/mol for formation of the

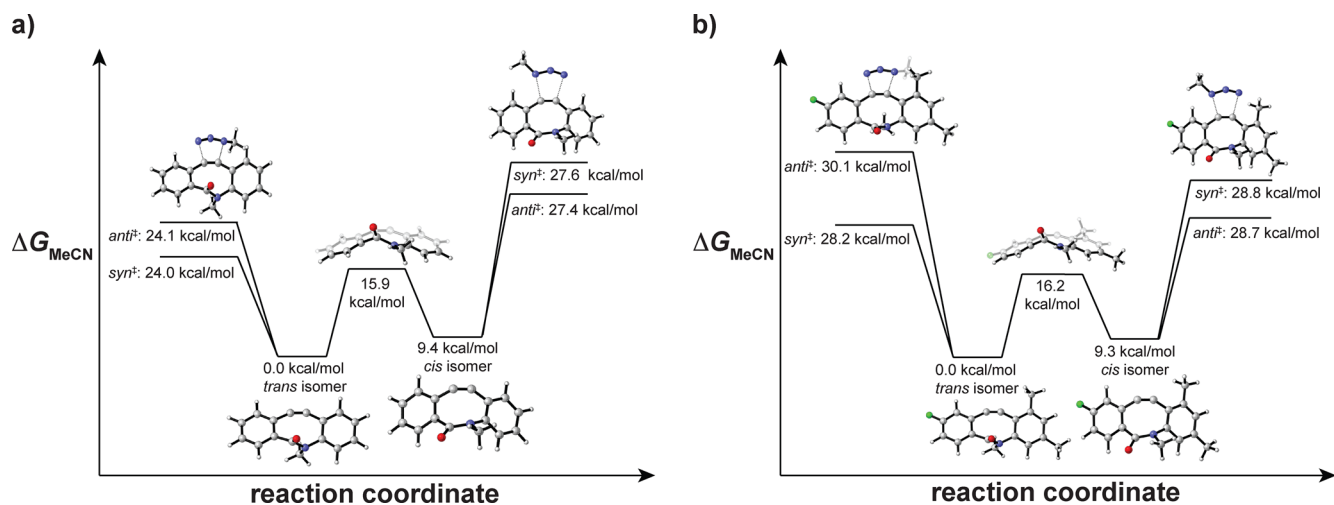


**Figure 7.** Under Curtin-Hammett conditions, BARAC's amide conformation influences reactivity and regioselectivity. (a) The reaction coordinate diagram displays calculated activation free energies for reaction of the parent BARAC compound **6** with methyl azide in acetonitrile. Also shown are the relative energies of *cis*-**6** and *trans*-**6** and the barrier to *cis/trans* interconversion. Transition state images show only the lowest-energy regioisomers. (b) Calculated values for the interconversion and reaction of analogue **15** with methyl azide in acetonitrile. Transition state images show only the lowest-energy regioisomers.



*syn*- and *anti*-regioisomers, respectively. Isomerization to and reaction of the *cis*-conformer have barriers of 27.4 (*anti*) and 27.6 (*syn*) kcal/mol, respectively. Because the energetic barrier to isomerization is significantly lower than the barrier to reaction, we hypothesize that BARAC isomerizes during the course of the cycloaddition. However, because the activation energy for reaction of the *trans*-isomer is lower than the activation energy for isomerization to and reaction of the *cis*-isomer, we conclude that BARAC (**6**) reacts mainly through the *trans*-isomer. As a result, the energetic barriers shown in Figure 7a, which predict a roughly 1:1 ratio of regioisomeric products, accurately predict the experimentally observed ratio of regioisomers (also 1:1).

The calculated barriers to *cis/trans* isomerization for both compounds **15** and **16** are about 16 kcal/mol, on par with that observed for the parent BARAC. Interestingly, however, for **15**, the transition state energies of the *trans*- and *cis*-isomers are much closer in energy than they are for those of the parent compound. Reaction of the *trans*-isomer of **15** displays activation energies of 28.2 (*syn*) and 30.1 (*anti*) kcal/mol, and reaction of the *cis*-isomer displays similar activation energies of 28.7 (*anti*) and 28.8 (*syn*) kcal/mol. Because the transition state energies of the *cis*- and *trans*-isomers are similar, we hypothesize that **15** may undergo the 1,3-dipolar cycloaddition with methyl azide by reacting through both the *cis* and the *trans* pathways. On the basis of this hypothesis and the aforementioned transition state energies, we calculate a *syn/anti* product ratio of 3:1 for **15**. Compound **16** also showed similar *trans* and *cis* transition state energetics, and gave a calculated *syn/anti* product ratio of 5:1. These values are close to the observed product ratios (3:1 and 2:1 *syn/anti* for **15** and **16**, respectively).

## CONCLUSION

We have performed a systematic analysis of the effects of strain and electronics on the reactivities of various cyclooctynes using the distortion/interaction model. We found that aryl ring substitution with electron-withdrawing and -donating groups produces only minor alterations in reactivity. The majority of the analogues tested did not display significant rate changes relative to that of the parent compound **6** for the reaction with benzyl azide. However, we did see a ~75% increase in reactivity for the difluorinated analogue **11**, which subsequent DFT calculations attributed to increased stabilizing interaction energy in the transition state of the reaction.

We observed more significant rate changes upon aryl substitution with groups capable of imposing steric hindrance in the transition state. Methyl-substituted analogues **15** and **16** and fluorine-substituted analogue **14**, which possess substituents at the flagpole position (ortho to the alkyne) displayed second-order rate constants between 2 and 3 orders of magnitude lower than that observed for parent BARAC. DFT data confirmed significantly increased transition state distortion energies for the reactions of these compounds with methyl azide. We also identified a correlation between total alkyne bond angle distortion and reactivity for the series of cyclooctynes shown in Table 1. Thus, computed alkyne bond angles as well as transition state distortion and interaction energies may be used in the informed design of cyclooctynes with tailored reactivities.

Analysis of BARAC's amide bond structure provided insight into its reactivity and regioselectivity with azides. X-ray structures of BARAC analogues provided evidence that

BARAC is able to modulate stability through amide bond rehybridization. As well, we found that BARAC's lactam has the *trans* configuration in crystal form. Computations confirmed that the *trans* conformation is energetically preferred to the *cis* conformation by 9.4 kcal/mol in acetonitrile and that this significant energetic difference may be in part a result of enhanced alkyne distortion upon isomerization to the *cis*-conformer (Figure 4). These data suggest that a *cis*-constrained BARAC analogue may display enhanced reactivity toward the azide as a result of enhanced strain.

Overall, our results show that DFT calculations can be a valuable resource in predicting the reactivity of potential new cyclooctynes. Accordingly, tools and trends summarized here should be useful for crafting new bioorthogonal reagents.

## ASSOCIATED CONTENT

### Supporting Information

Details of the syntheses of compounds **6–16**, full characterizations of **6–16**, kinetics data for the reactions of **6–16** with benzyl azide, computational (DFT) details, and X-ray crystallography data for **2**, **6**, **20**, and **21**. This material is available free of charge via the Internet at <http://pubs.acs.org>.

## AUTHOR INFORMATION

### Corresponding Author

[houk@chem.ucla.edu](mailto:houk@chem.ucla.edu); [crb@berkeley.edu](mailto:crb@berkeley.edu)

### Present Address

#Department of Chemistry and Biochemistry, University of Arizona, Tucson, AZ 85721.

### Notes

The authors declare no competing financial interest.

## ACKNOWLEDGMENTS

This work was funded by a grant to C.R.B. from the National Institutes of Health (GM058867). We are grateful to the National Science Foundation (CHE-0548209 to K.N.H.) for financial support of this research. Computer time was provided in part by the UCLA Institute for Digital Research and Education (IDRE) and the UC Shared Research Cluster Services South at San Diego Supercomputer Center, supported by the UC Office of the President. C.G.G. was supported by a predoctoral fellowship from the National Science Foundation. J.C.J. was supported by a postdoctoral fellowship from the American Cancer Society. E.M.S. was supported by a predoctoral fellowship from the American Chemical Society. We thank Dr. A. DiPasquale for solving crystal structures and Dr. C. Canlas for help with NMR kinetics experiments.

## REFERENCES

- (1) For reviews, see: (a) Sletten, E. M.; Bertozzi, C. R. *Angew. Chem., Int. Ed.* **2009**, *48*, 6974–6998. (b) Jewett, J. C.; Bertozzi, C. R. *Chem. Soc. Rev.* **2010**, *39*, 1272–1279. (c) Debets, M. F.; Van Berkel, S. S.; Dommerholt, J.; Dirks, A. J.; Rutjes, F. P. J. T.; Van Delft, F. L. *Acc. Chem. Res.* **2011**, *44*, 805–815. (d) Sletten, E. M.; Bertozzi, C. R. *Acc. Chem. Res.* **2011**, *44*, 666–676. (e) Debets, M. F.; Van der Doelen, C. W. J.; Rutjes, F. P. J. T.; Van Delft, F. L. *ChemBioChem* **2010**, *11*, 1168–1184.
- (2) (a) Bach, R. D. *J. Am. Chem. Soc.* **2009**, *131*, 5233–5243. (b) Meier, H.; Hanold, N.; Molz, T.; Bissinger, H. J.; Kolshorn, H.; Zountsas, J. *Tetrahedron* **1986**, *42*, 1711–1719. (c) Turner, R. B.; Jarrett, A. D.; Goebel, P.; Mallon, B. J. *J. Am. Chem. Soc.* **1973**, *95*, 790–792. (d) For a summary of the structures/properties of strained alkynes, see: Krebs, A.; Wilke, J. *Top. Curr. Chem.* **1983**, *109*, 189–233.

- (3) (a) Baskin, J. M.; Prescher, J. A.; Laughlin, S. T.; Agard, N. J.; Chang, P. V.; Miller, I. A.; Lo, A.; Codelli, J. A.; Bertozzi, C. R. *Proc. Natl. Acad. Sci. U.S.A.* **2007**, *104*, 16793–16797. (b) Chang, P. V.; Prescher, J. A.; Sletten, E. M.; Baskin, J. M.; Miller, I. A.; Agard, N. J.; Lo, A.; Bertozzi, C. R. *Proc. Natl. Acad. Sci. U.S.A.* **2010**, *107*, 1821–1826. (c) Laughlin, S. T.; Baskin, J. M.; Amacher, S. L.; Bertozzi, C. R. *Science* **2008**, *320*, 664–667. (d) Dehnert, K. W.; Beahm, B. J.; Huynh, T. T.; Baskin, J. M.; Laughlin, S. T.; Wang, W.; Wu, P.; Amacher, S. L.; Bertozzi, C. R. *ACS Chem. Biol.* **2011**, *6*, 547–552.
- (4) (a) Rostovtsev, V. V.; Green, L. G.; Fokin, V. V.; Sharpless, K. B. *Angew. Chem., Int. Ed.* **2002**, *41*, 2596–2599. (b) Tornøe, C. W.; Christensen, C.; Meldal, M. *J. Org. Chem.* **2002**, *67*, 3057–3064. (c) For a review of click chemistry see: Kolb, H. C.; Finn, M. G.; Sharpless, K. B. *Angew. Chem., Int. Ed.* **2001**, *40*, 2004–2021. For examples of *in vivo* Cu(I) catalysis see (d) Hong, V.; Steinmetz, N. F.; Manchester, M.; Finn, M. G. *Bioconjugate Chem.* **2010**, *21*, 1912–1916. (e) Soriano del Amo, D.; Wang, W.; Jiang, H.; Besanceney, C.; Yan, A. C.; Levy, M.; Liu, Y.; Marlow, F. L.; Wu, P. *J. Am. Chem. Soc.* **2010**, *132*, 16893–16899. (f) Besanceney-Webler, C.; Jiang, H.; Zheng, T.; Feng, L.; Soriano del Amo, D.; Wang, W.; Klivansky, L. M.; Marlow, F. L.; Liu, Y.; Wu, P. *Angew. Chem., Int. Ed.* **2011**, *50*, 8051–8056.
- (5) Agard, N. J.; Prescher, J. A.; Bertozzi, C. R. *J. Am. Chem. Soc.* **2004**, *126*, 15046–15047.
- (6) Agard, N. J.; Baskin, J. M.; Prescher, J. A.; Lo, A.; Bertozzi, C. R. *ACS Chem. Biol.* **2006**, *1*, 644–648.
- (7) (a) Ning, X.; Guo, J.; Wolfert, M. A.; Boons, G. J. *Angew. Chem., Int. Ed.* **2008**, *47*, 2253–2255. (b) Mbua, N. E.; Guo, J.; Wolfert, M. A.; Steet, R.; Boons, G. J. *ChemBioChem* **2011**, *12*, 1912–1921. (c) Debets, M. F.; Van Berkel, S. S.; Schoffelen, S.; Rutjes, F. P. J. T.; Van Hest, J. C. M.; Van Delft, F. L. *Chem. Commun.* **2010**, *46*, 97–99. (d) Jewett, J. C.; Sletten, E. M.; Bertozzi, C. R. *J. Am. Chem. Soc.* **2010**, *132*, 3688–3690.
- (8) (a) Chenoweth, K.; Chenoweth, D.; Goddard, W. A., III. *Org. Biomol. Chem.* **2009**, *7*, 5255–5258. (b) Ess, D. H.; Jones, G. O.; Houk, K. N. *Org. Lett.* **2008**, *10*, 1633–1636. (c) Schoenebeck, F.; Ess, D. H.; Jones, G. O.; Houk, K. N. *J. Am. Chem. Soc.* **2009**, *131*, 8121–8133.
- (9) Gold, B.; Shevchenko, N. E.; Bonus, N.; Dudley, G. B.; Alabugin, I. V. *J. Org. Chem.* **2012**, *77*, 75–89.
- (10) Calculated *p*-values (two-tailed, unpaired Student's *t*-test) comparing the second-order rate constants measured for compounds 7–9, 12, and 13 to that measured for 6 are  $0.5 > p > 0.001$ . The *p*-value calculated for compound 10 is  $p = 0.0001$ . *p*-values calculated for compounds 11 and 14–16 are  $p < 0.0001$ .
- (11) A disubstituted BARAC analogue with a fluorine atom at the position shown in compound 8 and a methoxy group at the position shown in compound 12 was synthesized, and its reactivity with benzyl azide was analyzed to determine the combined effects of electron-withdrawing and -donating groups on cyclooctyne reactivity. The calculated second-order rate constant was  $k = 1.1 \pm 0.1 \text{ M}^{-1} \text{ s}^{-1}$  for the reaction with benzyl azide in  $\text{CD}_3\text{CN}$  at rt—on par with rate constants observed for compounds 6–10, 12, and 13.
- (12) During the course of this work, a more extensive benchmarking of 1,3-dipolar cycloadditions to ethylene and acetylene was performed; see Lan, Y.; Zou, L.; Cao, Y.; Houk, K. N. *J. Phys. Chem. A* **2011**, *115*, 13906–13920. Through this work, more accurate methods and addition functionals for modeling these reactions were identified. The M06-2X functional was found to provide activation barriers that more closely matched higher-accuracy calculations. As a result, in addition to the B3LYP results in Figure 3c, M06-2X calculations have been performed on BARAC compounds 6 and 14–16 and are given in the SI. These activation energies deviate by 1.3–4.6 kcal/mol from energies calculated using the B3LYP functional. The conclusions are the same, except that M06-2X predicts all reactions to involve only the *trans*-isomer.
- (13) Ess, D. H.; Houk, K. N. *J. Phys. Chem. A* **2005**, *109*, 9542–9553.
- (14) De Graaff, R. A. G.; Gorter, S.; Romers, C.; Wong, H. N. C.; Sondheimer, F. *J. Chem. Soc., Perkin Trans. 2* **1981**, 478–480.
- (15) Sletten, E. M.; Bertozzi, C. R. *Org. Lett.* **2008**, *10*, 3097–3099.
- (16) (a) Cheong, P. H.-Y.; Paton, R. S.; Bronner, S. M.; Im, G.-Y. J.; Garg, N. K.; Houk, K. N. *J. Am. Chem. Soc.* **2010**, *132*, 1267–1269. (b) Im, G.-Y. J.; Bronner, S. M.; Goetz, A. E.; Paton, R. S.; Cheong, P. H.-Y.; Houk, K. N.; Garg, N. K. *J. Am. Chem. Soc.* **2010**, *132*, 17933–17944.
- (17) Codelli, J. A.; Baskin, J. M.; Agard, N. J.; Bertozzi, C. R. *J. Am. Chem. Soc.* **2008**, *130*, 11486–11493.
- (18) Kornmayer, S. C.; Rominger, F.; Gleiter, R. *Synthesis* **2009**, *15*, 2547–2552.
- (19) (a) Destro, R.; Pilati, T.; Simonetta, M. *J. Am. Chem. Soc.* **1975**, *97*, 658–659. (b) Kii, I.; Shiraishi, A.; Hiramatsu, T.; Matsushita, T.; Uekusa, H.; Yoshida, S.; Yamamoto, M.; Kudo, A.; Hagiwara, M.; Hosoya, T. *Org. Biomol. Chem.* **2010**, *8*, 4051–4055.
- (20)  $1 + i \cos \theta = 0$  where *i* = hybridization index. Anslyn, E. V.; Dougherty, D. A. *Modern Physical Organic Chemistry*; University Science Books: Mill Valley, CA, 2006; p 10.
- (21) Notably, Yoshida et al. recently reported that sterically hindered azides react more rapidly with cyclooctynes than unhindered azides. Their explanation for the energetic origins of this observation may also apply to our system. Yoshida, S.; Shiraishi, A.; Kanno, K.; Matsushita, T.; Johmoto, K.; Uekusa, H.; Hosoya, T. *Sci. Rep.* **2011**, *1*, 82.